CFRP dimensional stability investigations for use on the LISA mission telescope

J. Sanjuán, D. Korytov, A. Spector, and G. Mueller
University of Florida, Corner of Gale Lemerand Dr. and Museum Rd., Gainesville, FL 32611 USA

A. Preston and J. Livas
NASA Goddard Space Flight Center, Greenbelt, Maryland 20771 USA

A. Freise and G. Dixon
School of Physics and Astronomy, University of Birmingham, Edgbaston, Birmingham B15 2TT UK

(Dated: September 19, 2011)

Abstract

The Laser Interferometer Space Antenna (LISA) is a mission designed to detect low frequency gravitational-waves. In order for LISA to succeed in its goal of direct measurement of gravitational waves, many subsystems must work together to measure the distance between proof masses on adjacent spacecraft. One such subsystem, the telescope, plays a critical role as it is the laser transmission and reception link between spacecraft. Not only must the material that makes up the telescope support structure be strong, stiff and light, but it must have a dimensional stability of better than $1\,\mathrm{pm\,Hz^{-1/2}}$ at 3 mHz and the distance between the primary and the secondary mirrors must change by less than $2.5\,\mu$m over the mission lifetime. CFRP is the current baseline material, however, it has not been tested to the pico-meter level as required by the LISA mission. In this paper we present dimensional stability results, outgassing effects occurring in the cavity and discuss its feasibility for use as the telescope spacer for the LISA spacecraft.

PACS numbers: 04.80.Nn, 95.55.Ym, 07.87.+v, 81.05.U-

I. INTRODUCTION

The Laser Interferometer Space Antenna (LISA) is a proposed space mission conceived to detect gravitational waves (GWs) from astrophysical objects such as massive black holes and binary systems in the 0.1 mHz to 1 Hz frequency range [1–3]. LISA consists of a constellation of three *identical* spacecraft (SC) forming a triangle of approximately five million kilometers on a side which orbits the Sun in an Earth-like orbit about 20° behind the Earth. Each SC contains two proof masses (PMs) in *perfect* free-fall and laser interferometry is used to measure the distance between the PMs —see Fig. 1. In this manner GWs will be detected since they cause *geodesic deviations* in the free-falling PMs placed in the SC.

The expected PMs geodesic deviations due to GWs are extremely weak [1, 3]. Consequently, demanding requirements are imposed on all the LISA subsystems in order to ensure their detection. Each SC contains two main subsystems: the disturbance reduction system (DRS) and the interferometer measurement system (IMS) [4]. The main objective of the DRS is to maintain the free-fall of the PMs [5] that serves as a nominal reference point for the measurement of the inter-spacecraft distance. To keep the PMs in free-fall the DRS measures the position and orientation of the PMs with respect to the SC, applies control laws and commands micro-Newton thrusters such that the PM remains in its nominal position with respect to the SC [3, 5]. The DRS consists of an accelerometer (the so called Gravitational Reference Sensor, GRS) that measures the acceleration (by means of a capacitive sensor) between the PM and the SC, the drag-free attitude control system (DFACS) which applies the attitude control algorithms, and the thrusters which are driven by the DFACS and move the SC to keep it centered to the PM. Situated inside the spacecraft, the PMs are shielded from external effects such as solar radiation pressure. Obviously, the SC will be moved by such external effects, however, the DRS will correct the SC position to keep it centered to the PM. However, internal forces due to phenomena related to temperature fluctuations, magnetic field fluctuations, charging of the PM due to cosmic or solar radiation [6], microgravity effects, etc. are not shielded by the SC/DRS and thus they must be minimized by proper design regarding the mass distribution, the thermal balance, the magnetic cleanliness, etc. For this reason the required acceleration noise levels in terms of the linear spectral density (LSD) due to these forces in each PM compatible with GWs

detection have been set to

$$S_a^{1/2}(\omega) = 3 \times 10^{-15} \cdot \left[1 + \left(\frac{\omega/2\pi}{8\,\mathrm{mHz}}\right)^4\right]^{1/2} \left[1 + \left(\frac{0.1\,\mathrm{mHz}}{\omega/2\pi}\right)\right]^{1/2} \mathrm{m\,s^{-2}\,Hz^{-1/2}} \qquad (1)$$

in the frequency range from $0.1\,\mathrm{mHz} \leq \omega/2\pi \leq 1\,\mathrm{Hz}$. The performance of the DRS is a key element for the success of the mission. For this reason a technology readiness mission was approved by ESA and NASA. This is LISA Pathfinder (LPF) [5], scheduled to fly in 2014 and designed to put under test the DRS and meet the requirements given in Eq. (1) although relaxed by an order of magnitude both in acceleration noise ($30\,\mathrm{fm\,s^{-2}\,Hz^{-1/2}}$ instead of $3\,\mathrm{fm\,s^{-2}\,Hz^{-1/2}}$) and frequency band (from 1 mHz to 30 mHz).

The IMS will measure changes in the distances between the PMs by laser interferometry. The total IMS noise budget in terms of the LSD is [3]

$$S_{x,\mathrm{IMS}}^{1/2}(\omega) \leq 18 \times 10^{-12} \cdot \left[1 + \left(\frac{2.8\,\mathrm{mHz}}{\omega/2\pi}\right)^4\right]^{1/2} \mathrm{m\,Hz^{-1/2}},\ 0.1\,\mathrm{mHz} \leq \frac{\omega}{2\pi} \leq 1\,\mathrm{Hz} \qquad (2)$$

and consists primarly of laser shot noise[7], path-length noise[8], and measurement noise.

The overall noise curve (or sensitivity curve) of LISA is calculated from the noise sources of the DRS and IMS as [3]:

$$S_{x,\mathrm{LISA}}^{1/2}(\omega) = \sqrt{5}\frac{2}{\sqrt{3}}|T(\omega)| \left[S_{x,\mathrm{IMS}}(\omega) + \left(\frac{2}{\omega^2}\right)^2 S_{a,\mathrm{DRS}}(\omega)\right]^{1/2},\ 0.1\,\mathrm{mHz} \leq \frac{\omega}{2\pi} \leq 1\,\mathrm{Hz} \quad (3)$$

The term $\sqrt{5}$ comes from averaging the antenna response over the full sky. The term $2/\sqrt{3}$ ($= 1/\sin 60°$) is due to the fact that the arms of LISA do not form a right angle, but one of 60°. The other factor of two accounts for the presence of four PMs in the measurement in the difference between the two arms of the interferometer and the factor $1/\omega^2$ is the conversion from acceleration to position in the Fourier domain. $|T(\omega)|$ is the sensitivity function (the inverse of the transfer function) of LISA:

$$|T(\omega)| \simeq \left[1 + \left(\frac{\omega/2\pi}{0.012}\right)^2\right]^{1/2} \qquad (4)$$

The sensitivity of LISA will depend on the performance of these two subsystems. Essentially, internal noise sources will limit the PMs free-fall accuracy. These perturbations will dominate the lower frequency range (f <3 mHz) as their effect decays with ω^2 while noise in the IMS will dominate at higher frequencies due to quantum-limited displacement sensitivity.

A key element of the IMS is the telescope which simultaneously gathers the light coming from the far SC ($\sim$100 pW) and expands and collimates the small outgoing beam ($\simeq$2 W) and sends it to the far SC [4]. The distance between the two mirrors of the telescope is critical since it forms part of the science interferometer optical path. Therefore, any change in it translates directly into IMS path-length noise —see Fig. 2. The required stability of the distance between the two mirrors is [3]

$$S_{x,\mathrm{TS}}^{1/2}(\omega) \leq 10^{-12} \cdot \left[1 + \left(\frac{2.8\,\mathrm{mHz}}{\omega/2\pi}\right)^4\right]^{1/2} \mathrm{m\,Hz^{-1/2}}, \quad 0.1\,\mathrm{mHz} \leq \frac{\omega}{2\pi} \leq 1\,\mathrm{Hz} \qquad (5)$$

which corresponds to 5.5% of the total IMS budget —see Eq. (2). In addition to the stability requirement —Eq. (5)—, the distance between the two mirrors cannot change by more than $\sim$2.5 μm over the lifetime of the mission to prevent defocussing of the beam and thus wavefront distortion and optical efficiency degradation [9] —see Sec. IV.

The current LISA telescope baseline design consists of a two-mirror telescope with a two-lens ocular in an off-axis design (Schiefspiegler telescope) to avoid stray light sources and avoid obscuration of the beam path —see Fig. 3 [10, 11]. The primary and secondary mirrors are to be made of Zerodur. The diameter of the primary is 40 cm which results in an equivalent path-length noise due to shot noise of 8 pm $\mathrm{Hz}^{-1/2}$ (dominating noise for $f \geq$3 mHz). The telescope length is 60 cm and consists of a carbon fiber reinforced polymer (CFRP) cylinder-shaped spacer. CFRP consists of carbon fiber filaments in a matrix material which in most cases is a polymer such as an epoxy resin (and thus susceptible to outgassing). The mechanical, chemical, electrical and thermal properties of the CFRP depend on the production process, the fiber used and the matrix material. Advances in both fiber and resing technologies allow CFRP materials to be produced with a low coefficient of thermal expansion (CTE) [12], good vibration damping and excellent fatigue resistance. The telescope design would also include a re-focusing mechanism to allow for length changes that occur between on-ground testing and flight conditions due to the shrinking of the CFRP, and also to correct for dimensional changes during the mission. In addition an optical truss interferometer can be incorporated to the IMS to read out all potential length and alignment changes between the primary and the secondary mirrors for later corrections in post-processing [4, 10]. However, a very stable telescope structure could eliminate the need for an optical truss interferometer and the additional tunable telescope which would significantly simplify the design.

In this paper we discuss our experimental set-up to test the stability of the CFRP (independent of the geometry of the telescope spacer, i.e., using just an optical cavity made of CFRP) at the pico-meter level in the LISA frequency band, identify the noise sources present in the measurements, study the effect of outgassing on the material and discuss the viability of the CFRP to be used as the telescope support structure for the LISA mission.

The paper is organized as follows: Section II focuses on the experimental set-up together with the CFRP cavity construction process. Dimensional stability results are presented and discussed in Sec. III, outgassing measurements are presented in Sec. IV, and main conclusions and future prospects are summarized in Sec. V.

II. EXPERIMENTAL SET-UP

In order to determine the dimensional stability of the CFRP cavity, the set-up shown in Fig. 4 was used (see caption for details). A Pound-Drever-Hall (PDH) locking scheme was used to lock each laser to its respective cavity [13–15]. Two vacuum chambers, each consisting of a vacuum tank containing thermal shields, were used to house the cavities [9, 16, 17]. Tank 1 housed a Zerodur cavity (*reference* cavity) and contained five cylindrical layers of gold-coated stainless steel shells (to minimize heat transfer due to radiation) which were separated by macor spacers to minimize the heat flow between the thermal shields and the outer wall of the tank due to thermal conduction. Tank 2 housed the CFRP cavity and used five layers of aluminized polyethylene terephthalate (PET) also separated by macor spacers to achieve a benign thermal environment. The attenutation of the laboratory temperature fluctuations in the CFRP cavity is shown in Fig. 7 together with the theoretical transfer function —see Appendix A for details— and the required one to meet the requirements given in Eq. (5). The use of PET shells instead of gold-coated stainless steel in the CFRP cavity was only due to practical issues: the CFRP cavity was a temporary set-up while the Zerodur cavity set-up is a permanent one used for many other experiments. The difference between both is shown in Appendix A.

The relative dimensional stability of the CFRP was measured by beating the light from the laser locked to the CFRP cavity and the light from the laser locked to the Zerodur cavity which is assumed to be more stable than the CFRP (at least at low-frequency due to its very low CTE: $2 \times 10^{-8}\,\mathrm{K}^{-1}$). The frequency fluctuations of the beat-note were measured

by means of a frequency counter (HP 53132A) and they are

$$S_{\rm bn}(\omega) = \nu^2 \left[\frac{S_{\delta\ell_{\rm CFRP}}(\omega)}{\ell^2_{\rm CFRP}} + \frac{S_{\delta\ell_{\rm Zer}}(\omega)}{\ell^2_{\rm Zer}} \right] \quad [{\rm Hz^2\,Hz^{-1}}] \tag{6}$$

where $\ell_{\rm CFRP}$ is the length of the CFRP cavity and $S_{\delta\ell_{\rm CFRP}}$ its fluctuations. $\ell_{\rm Zer}$ is the length of the Zerodur cavity and $S_{\delta\ell_{\rm Zer}}$ its fluctuations and ν is the frequency of the laser (=281.95 THz, λ=1064 nm). Our goal was to determine $S_{\delta\ell_{\rm CFRP}}(\omega)$. In our set-up the lengths of both cavities are similar ($\ell \simeq$0.25 m), thus Eq. (6) becomes

$$S_{\rm bn}(\omega) \simeq \left(\frac{\nu}{\ell}\right)^2 \left[S_{\delta\ell_{\rm CFRP}}(\omega) + S_{\delta\ell_{\rm Zer}}(\omega)\right]. \tag{7}$$

Since the Zerodur cavity is supposed to be more stable than the CFRP, the dimensional stability of the latter can be estimated as:

$$S_{\delta\ell_{\rm CFRP}}(\omega) \simeq \left(\frac{\ell}{\nu}\right)^2 S_{\rm bn}(\omega) \quad [{\rm m^2\,Hz^{-1}}]. \tag{8}$$

At high frequencies, f >50 mHz, noise from electronics and optical components of the PDH set-up limits the measurement and thus Eq. (8) sets just an upper limit to the CFRP cavity stability measurement which is compatible with the stability we want to measure —see Fig. 13 for the noise curve of the Zerodur cavity.

In order to determine the absolute change in length of the CFRP cavity due to outgassing processes an absolute frequency reference was needed. To do this, a third laser was locked to a known hyperfine transition of the iodine molecule (P(54)32-0 line a_1) using the frequency modulation Doppler-free saturation spectroscopy technique [18–22] as shown in Fig. 5. Such transition is present around 532 nm. A non-linear crystal (Pp:MgLNO from HC Photonics) was used to generate the second harmonic of the 1064 nm laser. Laser 2 was kept locked to the CFRP cavity as in the set-up in Fig. 4. By monitoring the beat-note signal between the CFRP laser and the laser locked to the iodine transition the absolute length change of the CFRP cavity during the outgassing was measured.

A. CFRP cavity construction

A CFRP spacer was made at the University of Birmingham by the Center for Space and Gravity Research group. This group has experience in making CFRP structures for space-based missions and have had their parts flown on different missions including Hinode [23].

The CFRP cavity was designed to be stiff, strong and have a low CTE. The spacer is 230 mm in length and consists of a thin outer shell 200 mm in diameter and 5.5 mm thick that is used to provide additional structural support to an inner tube that has 45 mm outer diameter and 30 mm inner diameter. A set of struts 4.2 mm thick and spanning the length of the spacer connects the outer shell to the inner tube —see Fig. 6.

A multi-step process was used to make the CFRP spacer: the parts were fabricated, machined and epoxied together. Next a stress relief process based on three temperature cycles from 60°C to −20°C was performed. The spacer was cleaned and then vacuum baked at 100°C for one week. This step helps to accelerate outgassing of the epoxy. The rough/exposed parts were then machined and vacuum baked at 100°C for one week.

In addition to delivering the CFRP spacer, Zerodur tubes polished on one face were provided. One flat mirror and one mirror with a radius of curvature (ROC) of 1 m were optically contacted to the Zerodur tubes. The Zerodur mirror/plugs were then epoxied into the CFRP tube using Emerson & Cuming Eccobond 285 epoxy to form an optical cavity —see Fig. 6. The resulting cavity exhibited a linewidth of 160 kHz and a finesse, $\mathcal{F}$, of 4060.

III. DIMENSIONAL STABILITY MEASUREMENTS

This section presents the results obtained during the tests carried out to determine if the dimensional stability of the CFRP cavity meets the requirement imposed by the LISA mission —cf. Eq. (5). The results are summarized in Fig. 13. Prior to that the different sources of noise involved in the measurement are identified and quantified.

Two different mechanisms causing length fluctuations in the cavity have been identified as temperature fluctuations (this effect prevails for $f \lesssim 0.5$ mHz) and laser power fluctuations (from $\sim$1 mHz to $\sim$30 mHz). For frequencies higher than 50 mHz noise in the PDH technique from electronics, modulators, power fluctuations, etc. limit the sensitivity of the measurement.

A. Cavity temperature fluctuations and CTE estimation

The fluctuations of the CFRP cavity temperature cause length changes in the cavity due to the CTE of the material. In order to reduce this effect the cavity was placed in

a vacuum tank and it was surrounded by thermal shields —see Sec. II and Appendix A. However, this was not sufficient to attenuate properly the temperature fluctuations in the laboratory at frequencies lower than ∼0.2 mHz. Figure 7 (left panel) shows the PSDs of the temperature fluctuations in the laboratory and at the cavity. The right panel shows the modulus of the transfer function between laboratory and cavity temperature. The experimental transfer function can only be computed for frequencies lower than ∼0.2 mHz since at higher frequencies the temperature measurement inside the cavity is essentially dominated by electronic noise from the temperature read-out. The theoretical transfer function (see Appendix A) and the required one [considering the CTE given by Eq. (9)] to meet the LISA requirements are also shown.

The CTE is an important physical property since this ultimately sets the required thermal stability for the telescope structure in the LISA SC. It depends on the used components and the manufacturing process. We estimated the CTE by comparing the changes in the cavity temperature with the changes in the CFRP beat-note —see Fig. 8. The CTE was estimated using a linear least squares approach:

$$\alpha_{\mathrm{CFRP}} = \ell^{-1} \frac{\sum_{n=1}^{N} \Delta x[n] T[n]}{\sum_{n=1}^{N} T^2[n]} = 2.87 \times 10^{-6}\,\mathrm{K}^{-1} \tag{9}$$

where $x[n]$ is the beat-note measurement converted to length: $\Delta x = \frac{\ell}{\nu}\Delta\nu$, $T[n]$ is the temperature of the cavity and N ($=4 \times 10^5$) is the number of data points. All the changes in the beat-note due to temperature are ascribed to the CFRP cavity since the Zerodur CTE is about two orders of magnitude lower than the CFRP one. Figure 8 shows the measured length fluctuations of the CFRP (black trace) and the predicted length changes due to temperature fluctuations using the estimated CTE (red trace). The magenta trace shows the residual.

The estimated CTE implies that the required temperature stability in the LISA telescope assuming the real telescope length, 0.6 m, should be

$$S_{T,\mathrm{TS}}^{1/2}(\omega) \leq 0.58 \cdot \left[1 + \left(\frac{2.8\,\mathrm{mHz}}{\omega/2\pi}\right)^4\right]^{1/2} \mu\mathrm{K\,Hz}^{-1/2}, \quad 0.1\,\mathrm{mHz} \leq \frac{\omega}{2\pi} \leq 1\,\mathrm{Hz} \tag{10}$$

which is $450\,\mu\mathrm{K\,Hz}^{-1/2}$ at 0.1 mHz. The expected stability in the LISA telescope is $35\,\mu\mathrm{K\,Hz}^{-1/2}$ at 0.1 mHz and rolling-off as f^{-4} [24, 25]. However, this stability analysis considered Silicon Carbide (SiC) as the material, which exhibits a higher thermal conductivity and a different geometry. If CFRP is used instead the expected temperature stability

is about eight times worse due to the different thermal impedances. This yields an expected temperature stability of $280\,\mu\mathrm{K\,Hz^{-1/2}}$ at 0.1 mHz, which is still adequate to keep the length fluctuations of the telescope due to temperature changes within the LISA requirements if the CFRP telescope is used.

B. Mirror expansion due to laser power fluctuations

In the LISA mid-frequency range ($0.5\,\mathrm{mHz} \lesssim f \lesssim 30\,\mathrm{mHz}$) power fluctuations of the light hitting the cavity mirrors and the cavity itself cause length fluctuations due to thermal expansion of these elements. Figure 9 shows this effect.

To quantify this effect the power fluctuations in the transmitted light of the cavity, P_τ, were measured for two levels of incident light power in the cavity: $P_\tau \simeq 60\,\mu\mathrm{W}$ and $P_\tau \simeq 1.2\,\mathrm{mW}$.

The coherence function between power and beat-note data are shown in Fig. 11. Correlation is seen in two frequency regions. In the mid-frequency range (from 0.5 mHz to 30 mHz) power fluctuations cause thermal expansion of the elements of the cavity as explained below. Clearly, the correlation is weaker when the power is $60\,\mu\mathrm{W}$ since the effect in the mirrors/cavity is smaller. The correlation at higher frequencies between power fluctuations and beat-note fluctuations is ascribed to technical noise (electronics, modulators, etc.) of the PDH locking system. Such noise drives the laser frequency around the resonance of the cavity causing fluctuations which result in changes in the transmitted power which can be modeled as:

$$S^{1/2}_{x,\mathrm{el.}}(\omega) \simeq \frac{5\times 10^{-14}}{(\omega/2\pi)^{1/3}}\ \mathrm{m\,Hz^{-1/2}}. \tag{11}$$

Figure 11 (left) shows the LSD of the transmitted light power. The right panel shows the LSD of the beat-note measurement in units of length. The noise levels are clearly reduced in the mid-frequency range when P_τ=$60\,\mu\mathrm{W}$ since power fluctuations are proportional to the average power and thus the expansion of the mirrors/cavity due to heating effects is lower.

Cavity length fluctuations due to the thermal expansion of the mirrors and/or of the cavity itself can be expressed, in general, as

$$S_x(\omega) \simeq |H_{\mathrm{M}}(\omega)|^2 S_{P_\tau}(\omega) \tag{12}$$

where $H_{\mathrm{M}}(\omega)$ represents the transfer function between transmitted power fluctuations and

cavity length fluctuations. $H_{\rm M}(\omega)$ was estimated experimentally by applying a change in power (step function with ΔP=1.14 mW) while measuring the beat-note. The response of the system is shown in Fig. 12. Once the drift of the beat-note (caused by low-frequency temperature changes) is taken out the system can be modeled as a first-order low-pass filter, i.e.,

$$H_{\rm M}(\omega) \simeq \frac{\beta}{\tau i\omega + 1} \qquad [\mathrm{m\,W^{-1}}] \tag{13}$$

where β=5.8 μm W^{-1} and τ=3701 s.

The transfer function $H_{\rm M}(\omega)$ is used to estimate the noise apportioning of the power fluctuations in the beat-note measurements as described in Sec. III C.

C. Total noise apportioning

Using the results obtained in the previous sections, we can fully characterize the noise spectrum of the CFRP cavity. The length fluctuations in the whole measurement bandwidth are calculated as

$$S_x(\omega) = (\ell\alpha_{\rm CFRP})^2 S_{T,\rm CFRP}(\omega) + |H_{\rm M}(\omega)|^2 S_{P_\tau}(\omega) + S_{x,\rm el.}(\omega). \tag{14}$$

The results are shown in Fig. 13. Temperature fluctuations dominate for $f \leq$0.1 mHz for high power, and for $f \leq$0.4 mHz for low power. The expansion/contraction of the optical elements of the cavity due to power fluctuations is responsible for the noise between 0.1 mHz and 25 mHz when P_τ=1.2 mW but this effect is significantly reduced when the transmitted power is 60 μW: for $f >$ 3 mHz is negligible. At higher frequencies technical noise dominates both measurements and no difference is observed.

The blue-dashed trace in Fig. 13 is the telescope dimensional stability requirement for LISA —cf. Eq. (5)— which is met for the whole LISA frequency range when low power is used. At lower frequencies (out of the LISA band) the *goal* is not met due to temperature fluctuations in the cavity. However, temperature stability in the LISA telescope spacer should be better than the one available in the vacuum tanks. Consequently, the effect of the temperature on the cavity length will be milder —see Sec. III A.

In summary, the results in Fig. 13 show that the stability of the CFRP meets the LISA requirements. The length fluctuations of the cavity during the test are due to two understood mechanisms which should not be relevant for implementation on the LISA spacecraft: (i) in

LISA the temperature stability at low frequencies should be significantly better and (ii) the thermal expansion of the mirrors will be completely different in the LISA telescope. The second effect will require a detailed study once the design of the telescope is complete.

IV. OUTGASSING MEASUREMENTS

The CFRP cavity was made with an epoxy which is susceptible to outgassing under vacuum conditions as the ones expected in LISA. Such effect causes the material to shrink which could produce defocussing in the telescope if it is not well predicted and taken into account during the manufacturing process.

Outgassing effects were determined using the set-up described in Sec. II. The CFRP cavity was left in air for 17 days in an environment with a relative humidity around 50% in order to let it adsorb water vapor. After that the cavity was put in the vacuum chamber again and measurements started. The pressure was about 10^{-3} Pa after a couple of days and remained stable during the rest of the days. The beat signal was recorded for several hours each day. The results are shown in Fig. 14 for two different runs. The first run lasted for 30 days. The second run was taken in order to verify the results obtained in the first run and only 17 days of data were recorded since the behavior observed agreed with the first run. The red trace shows the measured change in length of the CFRP cavity. Together with the beat-note data the temperature of the cavity was also measured in order to correct for this effect. The blue trace shows the effect of the temperature on the cavity length. Finally, the contraction of the cavity due to outgassing (black and magenta traces) is estimated as

$$\Delta x_{\mathrm{outgas}}(t) = \Delta x_{\mathrm{total}}(t) - \ell \alpha_{\mathrm{CFRP}} \Delta T(t) \tag{15}$$

which can be modeled as a second-order system —see Fig. 14:

$$\Delta x_{\mathrm{outgas}}(t) = a(1 - e^{-t/\tau_1}) + b(1 - e^{-t/\tau_2}) \tag{16}$$

where $a = -1.53\,\mu$m, τ_1=1.8 day, $b = -4.89\,\mu$m and τ_2=18.7 day.

The CFRP cavity outgassing presents two behaviors: a fast one which has a time constant of 1.8 days and cause a change in length of $-1.53\,\mu$m and a slow one which has a time constant of 18.7 days and is responsible of a length change of $-4.89\,\mu$m. Thus the overall change in length is $-6.41\,\mu$m. Since the LISA SC will take 14 months [3] to reach its final orbit, all

of the outgassing will be done well in advance: about three months (assuming 5τ). Also the shrinkage of the telescope due to outgassing over the mission lifetime (5 years) would be about 1 pm and can be considered negligible. Taking into account the longer length of CFRP that will be used on the LISA SC, the total length change of the structure will be $\simeq$16.7 μm which clearly exceeds the required one: 2.5 μm.

The requirement of 2.5 μm is related to the wavefront error (WFE) introduced by the telescope due to defocussing, i.e., the position of the beam waist with respect to the telescope. The WFE requirement is set in order to keep the optical efficiency of the telescope about 85%. This property is specified by the Strehl ratio which is the ratio of the on-axis power from an optical system in the far field to the power the system would have if there were no wavefront aberrations, i.e., the on-axis power delivery efficiency of a real optical system compared to a perfect diffraction limited system. For small WFE it is given by

$$S = e^{-(2\pi\sigma/\lambda)^2} \tag{17}$$

where σ is the root mean square deviation of the wavefront and λ the wavelength. The LISA telescope efficieny has been set to ≥ 0.853 [3] which results in a WFE of $\sigma \simeq \lambda/20$ (=53 nm). Once the WFE budget is allocated we can estimate the maximum change in length of the telescope that causes such WFE. This has been done by simulations with Code V Optical Design Software. The obtained sensitivity of the WFE due to changes in the distance between the two mirrors, $\Delta\ell$, is [27]:

$$\frac{d\sigma}{d(\Delta\ell)} \simeq 21.65\,\mathrm{nm}\,\mu\mathrm{m}^{-1} \tag{18}$$

which means that the maximum $\Delta\ell$ to not exceed $\lambda/20$ is 2.5 μm. In our experiment we have estimated $\Delta\ell$=16.7 μm due to outgassing. This would cause a WFE of σ=361 nm ($\lambda/3$) resulting in $S = 0.01$. The equivalent path-length noise due to such effect is [3]

$$S_x^{1/2}(\omega) = 8\times10^{-12}\cdot\left(\frac{S_1}{S_2}\right)^{1/2} = 8\times10^{-12}\cdot\left(\frac{0.853}{0.01}\right)^{1/2} = 7.4\times10^{-11}\,\mathrm{m\,Hz^{-1/2}} \tag{19}$$

which is clearly unacceptable since the noise budget for the IMS is $18\times10^{-12}\,\mathrm{m\,Hz^{-1/2}}$.

The WFE depends critically on the position of the beam waist with respect to the telescope which is caused by the change in distance between the two mirrors —cf. Eq. (18). Therefore the telescope can be refocused on-flight by adjusting the position of two lenses. This is the so-called refocusing mechanism [3, 11]. However, the re-focusing mechanism can

correct only the telescope defocus, i.e., the parabolic part of the WFE. A change in the distance between the two mirrors in an off-axis design —see Fig. 3— causes a WFE that is not well approximated by a parabola, so minimizing the parabolic contribution only results in more aberration elsewhere and the number given in Eq. (18) will be higher (preliminary simulations have led to a factor of 16). On the contrary, the WFE in an on-axis design is cylindrically-symmetric and in any case well-approximated by a parabola, thus Eq. (18) remains the same. Consequently, an off-axis design is more sensitive than an on-axis design to an on-axis length change. For this reason an on-axis design made of Silicon Carbide (SiC) is also being investigated which will be less sensitive to de-focus and, pressumably, it will exhibit less outgassing since SiC is much less porous than CFRP. We are currently working on these matters, and will report shortly on progress elsewhere.

In addition, more investigations concerning the CFRP outgassing are required since a fair degree of predictability of the shrinkage of the telescope spacer can be taken into account to have a design that after the outgassing effects have the right distance between the two mirrors.

V. DISCUSSION

The telescope in LISA is a key element of the IMS since it is in charge of transmitting and receiving the light between the different SC. Very demanding requirements have been set to the dimensional stability of the telescope, $1\,\mathrm{pm\,Hz^{-1/2}}$, in order to guarantee GW detection. The current telescope baseline consists of a CFRP cylinder structure (60 cm in length) holding the two mirrors of the telescope. We have investigated the CFRP dimensional stability by using a CFRP cavity of length 23 cm.

The dimensional stability of the CFRP material tested meets the LISA telescope requirement if the temperature stability is better than $450\,\mu\mathrm{K\,Hz^{-1/2}}$ at 0.1 mHz since we have determined its CTE to be $2.87\times10^{-6}\,\mathrm{K^{-1}}$. Another source of noise was detected in the mid-frequency range due to the thermal expansion of the cavity mirrors caused by power fluctuations of the laser. Such effect was identified and mitigated in order to reach the LISA requirements. In LISA the mirrors will be completely different and dedicated investigations on that matter should be carried out. Although the dimensional stability of the material was tested at room temperature, the expected operating temperature of the telescope will

be around $-70\,^{\circ}$C and further investigations at this temperature should be perfomed in the future. Despite this, the results at room temperature provide a good estimation of the behavior of the material since drastic differences are not foreseen at $-70\,^{\circ}$C.

Another requirement for the telescope is the overall length stability which has to change less than $2.5\,\mu$m over the mission lifetime in order to avoid wavefront distortion and keep the optical efficiency of the telescope about 85%. Outgassing of the material causes length changes of the cavity. We have performed tests to identify the outgassing behavior of the CFRP cavity and determined the shrinkage of the cavity to be $6.41\,\mu$m which scaled with the actual LISA telescope length would be about $17\,\mu$m. Such length change is much larger than the required $2.5\,\mu$m and thus care must be taken when designing and constructing the telescope. Also this indicates the need of a re-focusing mechanism on-board the LISA SC in order to correct for this effect.

In addition, a more LISA-like structure needs to be tested in the future. The outer shell of the cavity confines the inner cylinder to prevent twisting or bending, but results in a diameter that is too large to be used in the LISA SC. Further testing will need to be done on a structure with dimensions that will be used on the LISA SC to determine if there is any twisting or bending that is produced from the material outgassing in a non-uniform fashion.

Appendix A: Thermal insulator transfer function derivation

In this appendix we derive the theoretical transfer function of the thermal insulating system installed in the vacuum tanks housing the cavities —see Fig. 15. To do so we have assumed that heat transfer is only due to radiation. If conductive thermal links are minimized their effect should be small.

Radiation heat transfer from one surface i to another j for spherical grey bodies (we approximate the closed cylinders to spheres for simplicity: the cylinders are $\simeq$0.85 m in height and $\simeq$1 m in diameter thus the approximation is justified) is [28]:

$$\dot{q}_{i\to j} = \frac{\sigma A_j (T_i^4 - T_j^4)}{\frac{1}{\varepsilon_j} + \frac{1-\varepsilon_i}{\varepsilon_i}\left(\frac{r_j}{r_i}\right)^2} \tag{A1}$$

where $\sigma = 5.67\times10^{-8}\,\mathrm{W\,m^{-2}\,K^{-1}}$, A_j is the area of the body j, $r_{i,j}$ the radius of the spheres and $\varepsilon_{i,j}$ their emissivities. The temperature increase of the body j is:

$$\dot{q}_{i\to j} = C_j \dot{T}_j(t) = m_j c_{j,\mathrm{h}} \dot{T}_j(t) \tag{A2}$$

where m_j and $c_{j,\mathrm{h}}$ are the mass and specific heat, respectively. Equating Eqs. (A1) and (A2) yields

$$\frac{\sigma A_j[T_i^4(t) - T_j^4(t)]}{\beta_{ij}} = C_j \dot{T}_j(t) \tag{A3}$$

where for notation simplicity we define β_{ij} as

$$\beta_{ij} \equiv \frac{1}{\varepsilon_j} + \frac{1-\varepsilon_i}{\varepsilon_i}\left(\frac{r_j}{r_i}\right)^2 \tag{A4}$$

In order to be able to solve the differential equation given in (A3) we linearize the terms $T_{i,j}^4(t)$, i.e.,

$$T_k^4(t) = T_{0,k}^4 + 4T_{0,k}^3 \Delta T_k(t) \tag{A5}$$

where $T_{0,k}$ is the initial temperature and $\Delta T_k(t) = T_k(t) - T_{0,k}$. The temperature fluctuations in the system are small thus the linear approximation is justified (the error in the temperature range from 300 K to 305 K is less than 0.2%). Substituion of Eq. (A5) into Eq. (A3) and assuming $T_{0,i} = T_{0,j} = T_0$ (both bodies are initially at the same temperature) leads to

$$\frac{\sigma A_j}{\beta_{ij}} 4T_0^3[\Delta T_i(t) - \Delta T_j(t)] = C_j \frac{d}{dt}\Delta T_j(t) \tag{A6}$$

The transfer function can be easily found by using the Laplace transform of Eq. (A6):

$$\frac{\sigma A_j}{\beta_{ij}} 4T_0^3[\widetilde{\Delta T}_i(s) - \widetilde{\Delta T}_j(s)] = C_j s\widetilde{\Delta T}_j(s) + \Delta T_j(t=0) \tag{A7}$$

where $\widetilde{\Delta T}_{i,j}(s) \equiv \mathcal{L}[\Delta T_{i,j}(t)]$ and the initial condition is set to zero. The transfer function between both bodies is simply the ratio between $\widetilde{\Delta T_j}$ and $\widetilde{\Delta T_i}$ and we use $s = \mathbf{i}\omega$ to transform from the Laplace domain to the Fourier domain:

$$H(\omega) = \frac{\widetilde{\Delta T}_j(\omega)}{\widetilde{\Delta T}_i(\omega)} = \frac{1}{\frac{1}{2\pi f_{\mathrm{cut-off}}}\mathbf{i}\omega + 1} \tag{A8}$$

which corresponds to a low-pass filter of first order with

$$f_{\mathrm{cut-off}} = \frac{1}{2\pi}\frac{4\sigma A_j T_0^3}{C_j \beta_{ij}} \tag{A9}$$

The insulating system in the CFRP tank contains five layers of PET —see Fig. 15, therefore we need to calculate six transfer functions H_k (k=1,2,...,6) where $H_1(s)$ stands for the transfer function between the aluminum wall of the tank and the first PET layer. $H_{2,3,4,5}(s)$ represent the transfer functions between the PET layers. $H_6(s)$ is the transfer

function from the last PET layer and the cavity (where the heat capacitance of the stand has to be taken into account). Obviously the same calculations can be done for the stainless-steel gold coated shields used for the Zerodur cavity.

Figure 16 shows the estimated transfer functions using the values given in Table I. The cut-off frequencies of $H_{1,\ldots,5}$ for the CFRP tank are $\simeq$0.2 mHz whereas for the Zerodur tank are $\simeq$6.6 μHz. The difference is essentially due to the larger mass of the stainless steel shields which pushes the cut-off frequency to the micro-Hertz range. H_6 adds a pole at very low-frequency: 0.81 μHz and 4.3 μHz for the CFRP tank and Zerodur tank, respectively. This pole appears due to the large mass of the cavity and the stand together. The comparison between the measured CFRP transfer function and the theoretical one is shown in Fig. 7.

The analysis shown here is a very simplified model of the actual one, for instance, conductive links have not been taken into account and very simplified geomtries have been used for the radiative model. However, it is still useful to obtain an approximation of the ideal transfer function of the system. As shown in Fig. 7 the theoretical and experimental transfer functions are in good agreement at low frequencies ($f \leq$0.2 mHz). For higher frequencies the experimental transfer function cannot be measured due to inherent noise of the temperature sensors.

---

[1] LISA Study Team, *LISA for the detection and observation of gravitational waves. Pre-phase A*, Tech. Rep. 244 (Max Plank für Quantenoptik, 1998).

[2] K. Danzmann, Adv. in Space Res. **32**, 1233 (2003).

[3] LISA International Science Team (LIST), *LISA: Unveiling a hidden Universe*, Tech. Rep. (European Space Agency, 2011).

[4] O. Jennrich, Class. Quantum Grav. **26**, 153001 (2009).

[5] M. Armano, M. Benedetti, J. Bogenstahl, D. Bortoluzzi, P. Bosetti, N. Brandt, A. Cavalleri, G. Ciani, I. Cristofolini, A. Cruise, K. Danzmann, I. Diepholz, G. Dixon, R. Dolesi, J. Fauste, L. Ferraioli, D. Fertin, W. Fichter, M. Freschi, A. García, C. García, A. Grynagier, F. Guzm'an, E. Fitzsimons, G. Heinzel, M. Hewitson, D. Hollington, J. Hough, M. Hueller, D. Hoyland, O. Jennrich, B. Johlander, C. Killow, A. Lobo, D. Mance, I. Mateos, P. McNamara, A. Monsky, D. Nicolini, D. Nicolodi, M. Nofrarias, M. Perreur-Lloyd, E. Plagnol,

G. Racca, J. Ramos-Castro, D. Robertson, J. Sanjuán, M. Schulte, D. Shaul, M. Smit, L. Stagnaro, F. Steier, T. Sumner, N. Tateo, D. Tombolato, G. Vischer, S. Vitale, G. Wanner, H. Ward, S. Waschke, V. Wand, P. Wass, W. Weber, T. Ziegler, and P. Zweifel, Class. Quantum Grav. **26**, 094001 (2009).

[6] P. Cañizares, A. Conchillo, E. García-Berro, L. Gesa, C. Grimani, I. Llori, A. Lobo, I. Mateos, M. Nofrarias, J. Ramos-Castro, and J. Sanjuán, Class. Quantum Grav. **26**, 094005 (2009).

[7] The received power from the far SC is about 100 pW which is equivalent to pathlength noise of $8\,\mathrm{pm\,Hz^{-1/2}}$.

[8] Any distance fluctuation between the different optical components will mimic the effect of GWs on the PMs.

[9] A. Preston, *Stability of materials for use in space-based interferometric missions*, Ph.D. thesis, University of Florida (2010).

[10] M. Sallusti, P. Gath, D. Weise, M. Berger, and H. R. Schulte, Class. Quantum Grav. **26**, 094015 (2009).

[11] D. Weise, *Telescope Subsystem Specification LISA-ASD-RS3300*, Tech. Rep. (EADS Astrium, 2008).

[12] T. Schuldt, M. Gohlke, D. Weise, U. Johann, and C. Braxmaier, Optomechatronic Technologies (ISOT), 2010 International Symposium on (IEEE)(2009).

[13] R. W. P. Drever, J. L. Hall, F. V. Kowalski, J. Hough, G. M. Ford, M. A. J, and H. Ward, Appl. Phys. B **31**, 97 (1983).

[14] E. D. Black, Am. J. Phys. **69**, 79 (2001).

[15] D. Shoemaker, A. Brillet, C. Nary Man, O. Crégut, and G. Kerr, Opt. Lett. **14**, 609 (1989).

[16] R. Cruz, *Development of the UF LISA benchtop simulator for the time delay interferometry*, Ph.D. thesis, University of Florida (2006).

[17] R. Cruz, J. I. Thorpe, A. Preston, R. Delgadillo, M. Hartman, S. Mytrik, A. Worley, G. Boothe, R. G. Sridhar, S. Klimenko, D. B. Tanner, and G. Mueller, Class. Quantum Grav. **23**, S751 (2006).

[18] A. Arie, S. Schiller, E. K. Gustafson, and R. L. Byer, Opt. Lett. **17**, 1204 (1992).

[19] G. C. Bjorklund, M. D. Levenson, W. Lenth, and C. Ortiz, Appl. Phys. B **32**, 145 (1983).

[20] V. Leonhardt and J. B. Camp, Appl. Opt. **45**, 4142 (2006).

[21] J. L. Hall, M. Long-Scheng, M. Taubman, B. Tiemann, F. L. Hong, O. Pfister, and J. Ye,

IEEE Trans. Instr. Meas. **48**, 583 (1999).

[22] B. Argence, H. Halloin, O. Jeannin, P. Prat, O. Turazza, E. de Vismes, G. Auger, and E. Plagnol, Phys. Rev. D **81**, 082002 (2010).

[23] J. L. Culhane, L. K. Harra, A. M. James, K. Al-Janabi, L. J. Bradley, R. A. Chaudry, K. Rees, J. A. Tandy, P. Thomas, M. C. R. Whillock, B. Winter, G. A. Doschek, C. M. Korendyke, C. M. Brown, S. Myers, J. Mariska, J. Seely, J. Lang, B. J. Kent, B. M. Shaughnessy, P. R. Young, G. M. Simnett, C. M. Castelli, S. Mahmoud, H. Mapson-Menard, B. J. Probyn, R. J. Thomas, J. Davila, K. Dere, D. Windt, J. Shea, R. Hagood, R. Moye, H. Hara, T. Watanabe, K. Matsuzaki, T. Kosugi, V. Hansteen, and O. Wikstol, Solar Physics **243**, 19 (2007).

[24] A. Davis, *LISA quadpod spacer thermal study final report*, Tech. Rep. (Edge Space Systems, 2008).

[25] H. Peabody and S. M. Merkowitz, AIP Conf.Proc. **873**, 204 (2006).

[26] J. Livas, Personal communication (2011).

[27] J. Livas, *Preliminary Telescope Requirements and Spacer Design*, Tech. Rep. LISA Project internal report LISA-MSE-TN, Version 0, Issue 3 (NASA Goddard Space Flight Center, 2011).

[28] F. Incropera and D. De Witt, *Fundamentals of heat transfer* (John Wiley & Sons (New York), 1981).

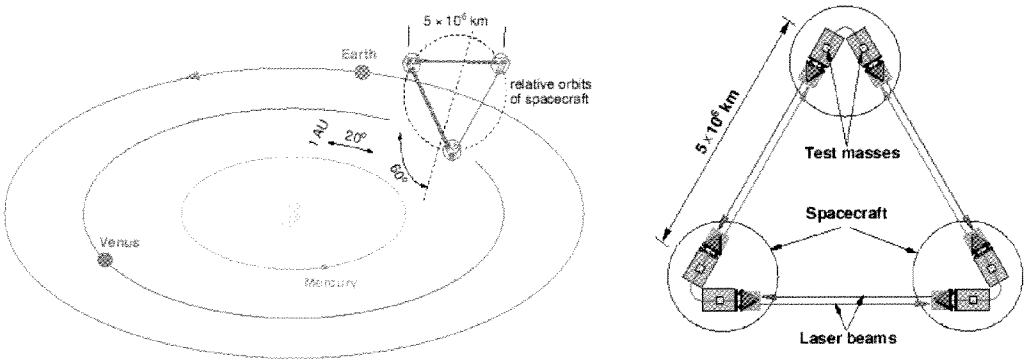

FIG. 1. Left: LISA orbit. Right: LISA's equilateral triangle constellation. (Not to scale).

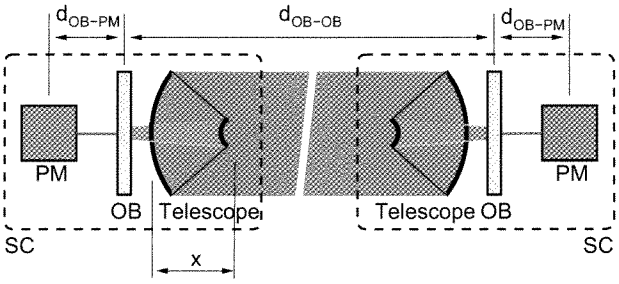

FIG. 2. LISA arm scheme. The distance between the PMs must be measured at the pico-meter level in the milli-Hertz range in order to ensure GW detection. x=0.6 m, $d_{\mathrm{OB-PM}} \simeq 0.05$ m and $d_{\mathrm{OB-OB}} \simeq 5$ Gm (OB stands for optical bench). Distance fluctuations between the two mirrors of the telescope translate directly into path-length noise and thus spoil the LISA sensitivity. The noise budget assigned to this effect is given by Eq. (5).

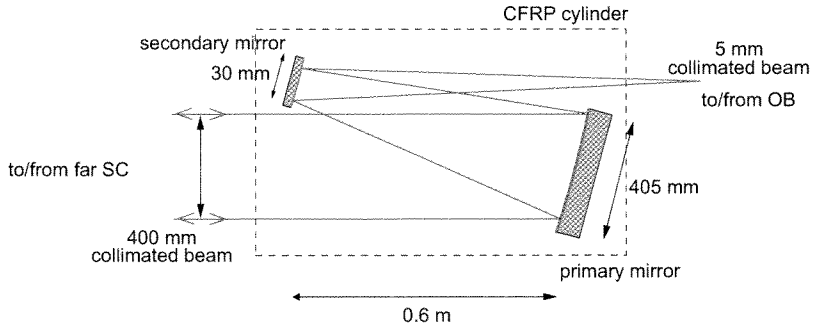

FIG. 3. Scheme of the LISA telescope current baseline design. The cylinder-shaped spacer (0.55 m diameter and 1 m length) is made of CFRP [10].

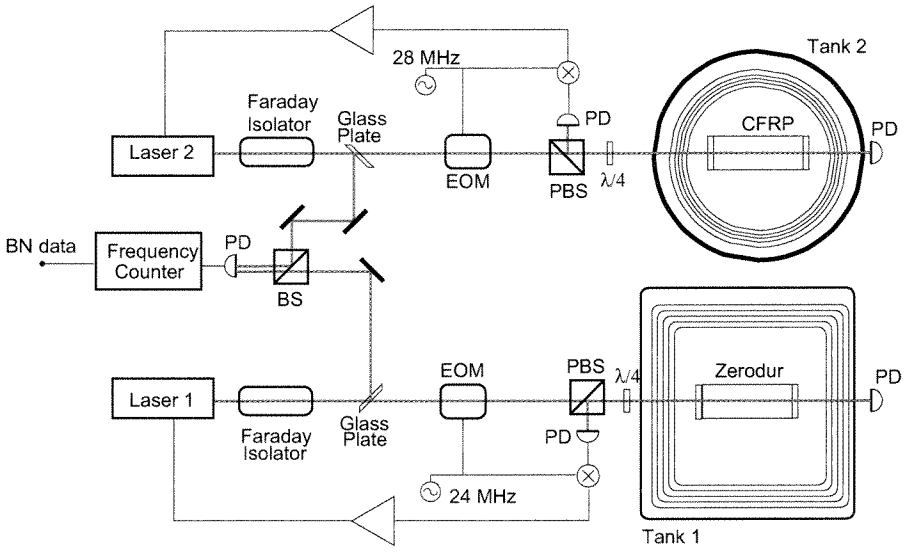

FIG. 4. Set-up used to determine the relative dimensional stability of the CFRP cavity. All the lasers of the set-up are Nd:YAG with a wavelength of 1064 nm. Each laser is locked to its respective cavity using the PDH technique. In this manner the frequency of the laser tracks the length fluctuations of the cavity. EOM: electro-optical modulator, BS: power beam splitter, PBS: polarizing beam splitter, PD: photo-detector and $\lambda/4$: quarter-wave plate.

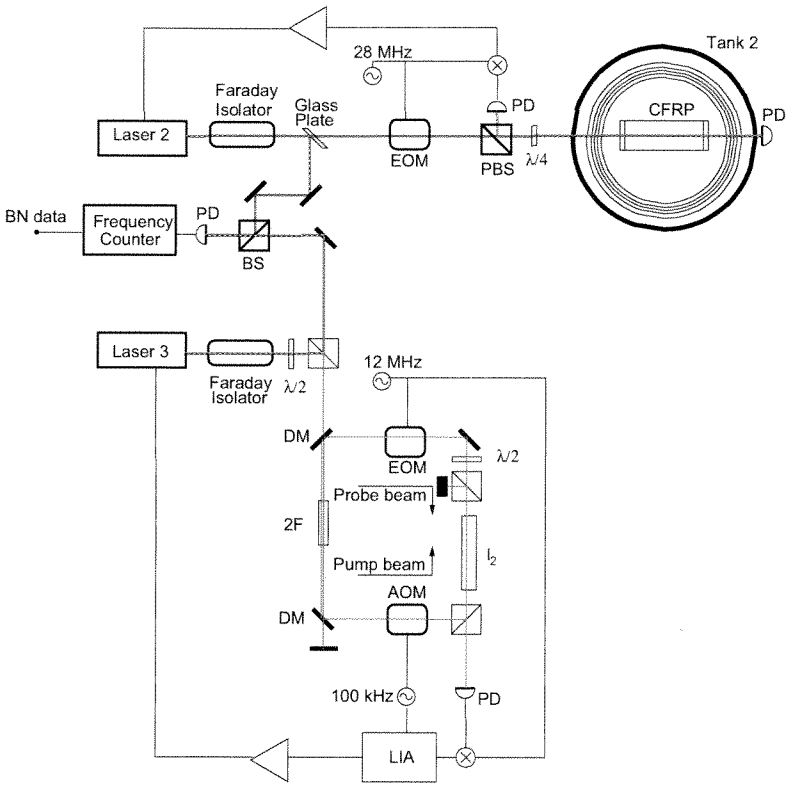

FIG. 5. Set-up used to determine the absolute length changes of the CFRP cavity during the outgassing process. All the lasers of the set-up are Nd:YAG with a wavelength of 1064 nm. Laser 3 is locked to a hyperfine transition of the iodine molecule using the frequency modulation Doppler-free saturation spectroscopy technique to provide an absolute frequency reference. Laser 2 is locked to the CFRP cavity using the PDH technique. DM: dichroic mirror, AOM: acoustic-optical modulator, LIA: lock-in amplifier, $\lambda/2$: half-wave plate, I_2: iodine molecules and 2F is a non-linear crystal (Pp:MgLNO) that creates the second harmonic of the Nd:YAG laser.

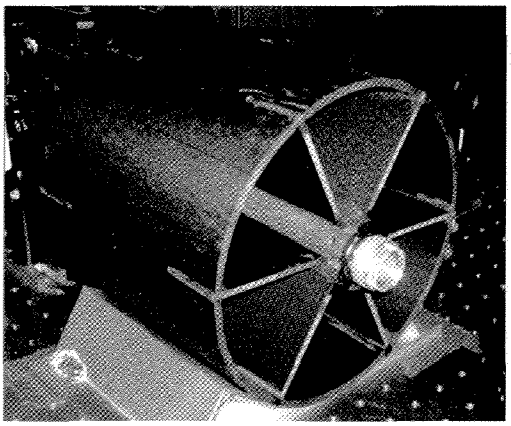

FIG. 6. Completed CFRP cavity with Zerodur/mirror plugs epoxied into place. The structure is 230 mm long. The outer shell is 200 mm in diameter and 5.5 mm thick. The inner tube has 45 mm outer diameter and 30 mm inner diameter. The struts are 4.2 mm thick.

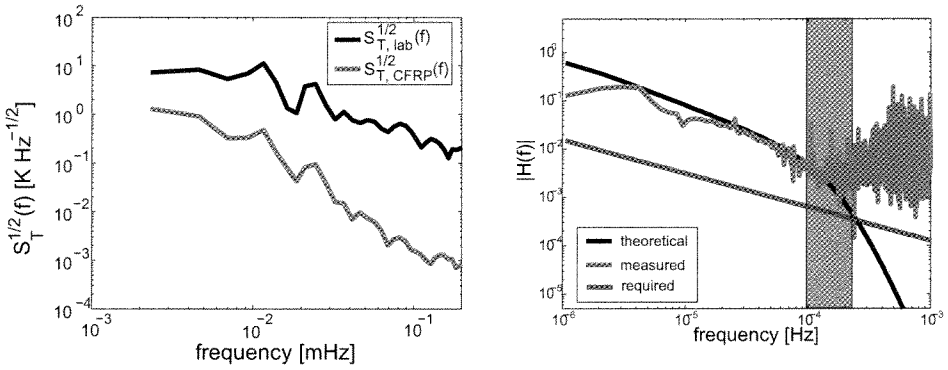

FIG. 7. Left: laboratory temperature fluctuations (black trace) and cavity temperature fluctuations (red trace). Right: transfer function between laboratory and cavity temperature fluctuations. Black trace is the theoretical one —see Appendix A. The red trace is the measured one and the blue one is the required to meet the requirements. The pink area shows the frequency range where the temperature stability is not good enough for our experiments in the LISA band.

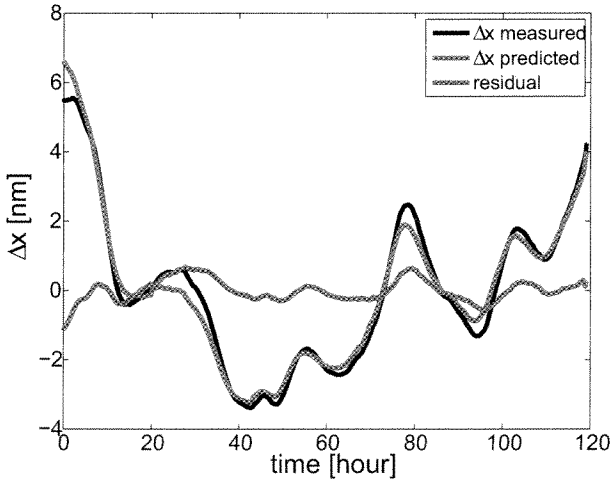

FIG. 8. Measured length fluctuations (black trace) and predicted ones due to temperature fluctuations (red trace) using the estimated CTE.

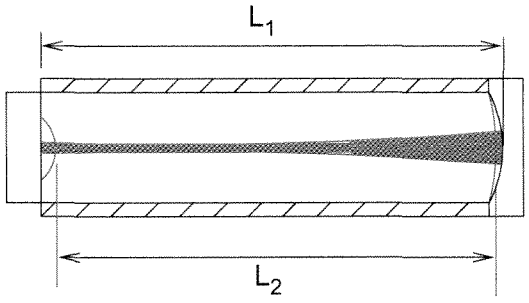

FIG. 9. Expansion/contraction of the mirrors due to the power build up in the cavity. L_1 is the length of the cavity at a given temperature and in absence of light. L_2 is the length of the cavity when the laser is in resonance with the cavity. The temperature of the mirrors increases due to absorption and, consequently, they expand due to their CTE. The length of the mirrors of the cavity (and the cavity itself) reaches a steady-state for a given power built up in the cavity. If the power fluctuates the length of the mirrors fluctuates accordingly.

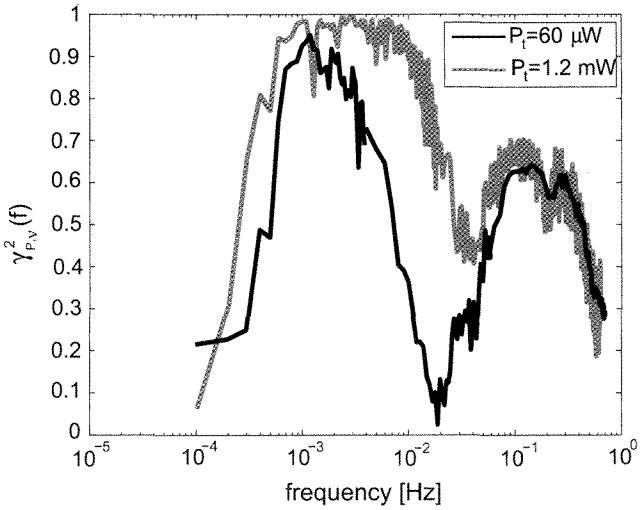

FIG. 10. Coherence function between transmitted power, P_τ, and beat-note for P_τ=60 μW and P_τ=1.2 mW.

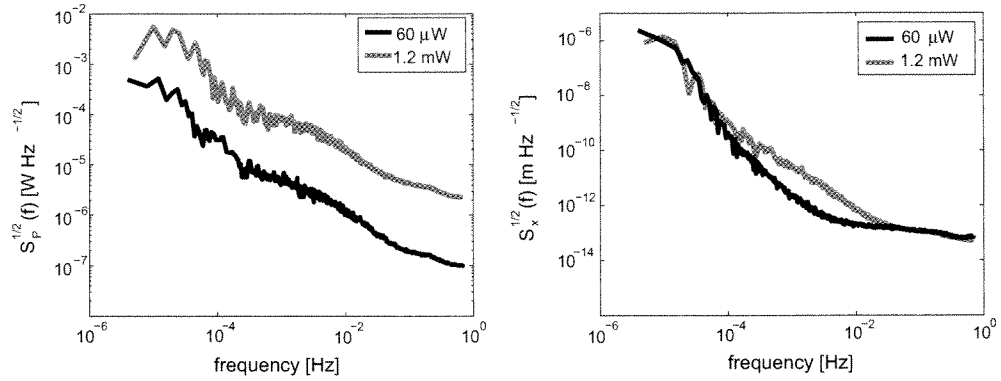

FIG. 11. Left: linear spectral density of the transmitted light power. Right: linear spectral density of the length fluctuations of the cavity. The noise in the mid-frequency range is significantly reduced when using low power.

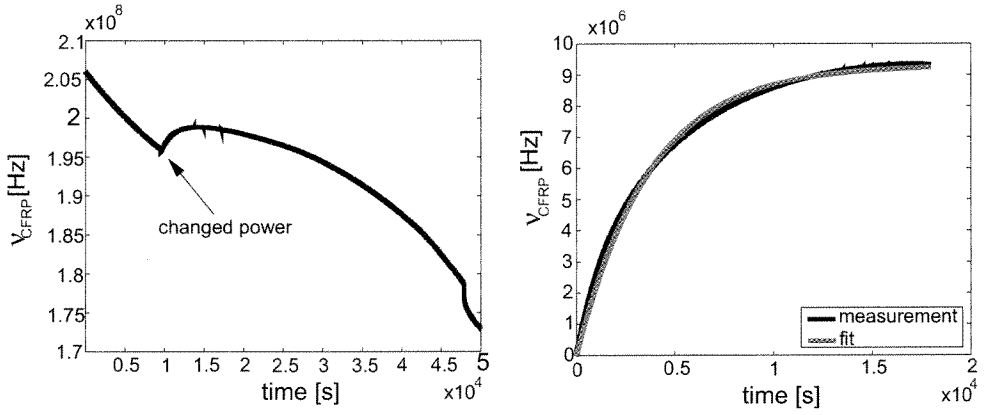

FIG. 12. Left: beat-note response after changing power going into the cavity by 1.14 mW. Right: Once the drift of the beat-note (caused by low-frequency temperature fluctuations) is removed a first-order response is clearly seen. The black trace is the measured signal while the red trace is the fit —see Eq. (13).

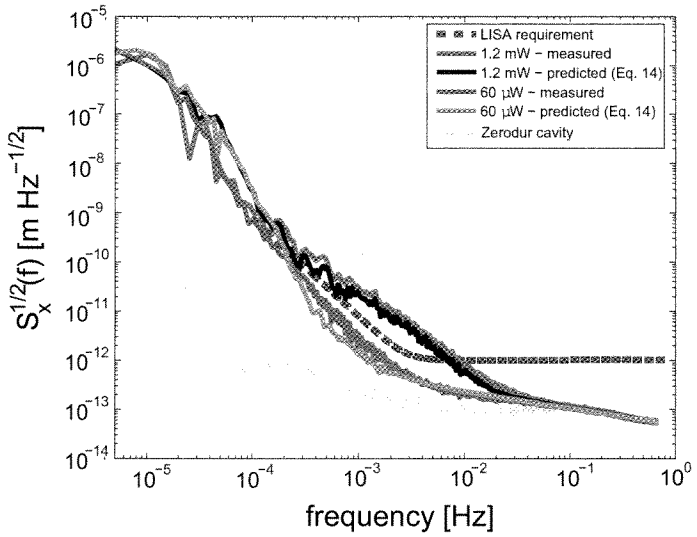

FIG. 13. Stability results for two different power levels: 1.2 mW (red trace) and 60 μW (magenta trace). The predicted stability using Eq. (14) is also shown for the two different measurements (black and green traces). The blue-dashed line is the LISA telescope requirement. The discrepancy for $f \lesssim 0.1$ mHz is because the temperature and the beat-note data were not measured simultaneously and the temperature fluctuations during the beat-note measurement were lower than the ones during the temperature measurements. The yellow trace shows the Zerodur cavity stability measurements which sets the noise levels of the CFRP stability measurements.

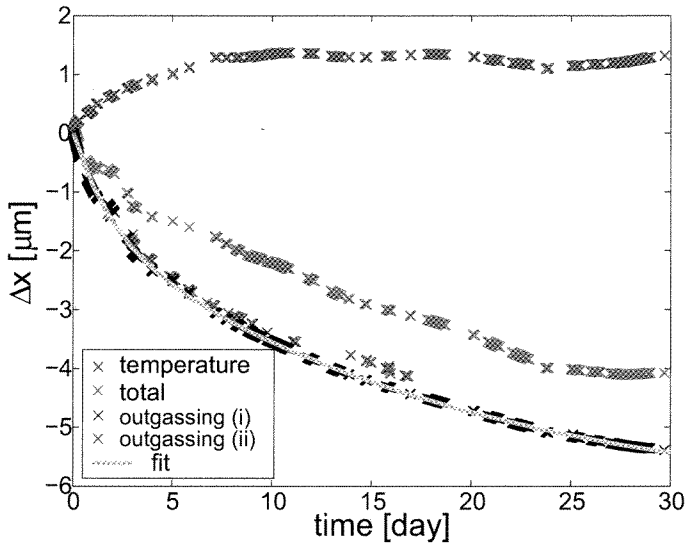

FIG. 14. Red trace: the measured length change of the CFRP cavity. Black and magenta traces: length change in the cavity due to outgassing, i.e., after removing the effect of the temperature (blue trace). The temperature data and total length change traces correspond to the outgassing data given by the black trace. The same process was done to the magenta trace although the temperature and total length change are not shown in the plot for clarity.

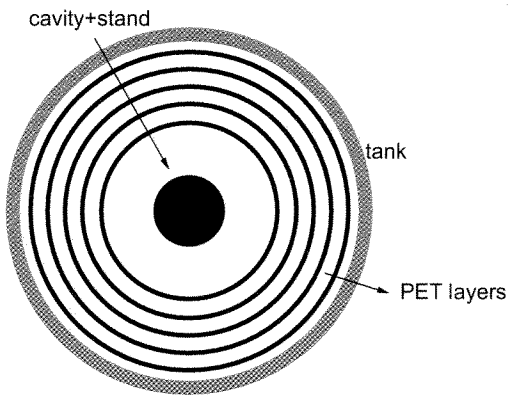

FIG. 15. Thermal insulator concept. The cavity is placed inside the tank sitting on top of a stand and surrounded by PET shields. The PET shields are closed cylinders. *Idem* for the Zerodur cavity but with stainless-steel gold coated shields instead of PET ones.

TABLE I. Parameters used to calculate $f_{\mathrm{cut-off}}$ for the CFRP tank and Zerodur tank.

	Tank CFRP	PET shields	CFRP+stand	Tank Zerodur	Stainless Steel shields	Zerodur+stand
C [J kg^{-1}]	—	230	48 000	—	2 800	5 200
ε	0.35	0.03	1	0.35	0.028	0.9
r [m]	0.75	0.5	0.12	0.55	0.4	0.04
A [m^2]	—	2.7	0.17	—	1.4	0.03

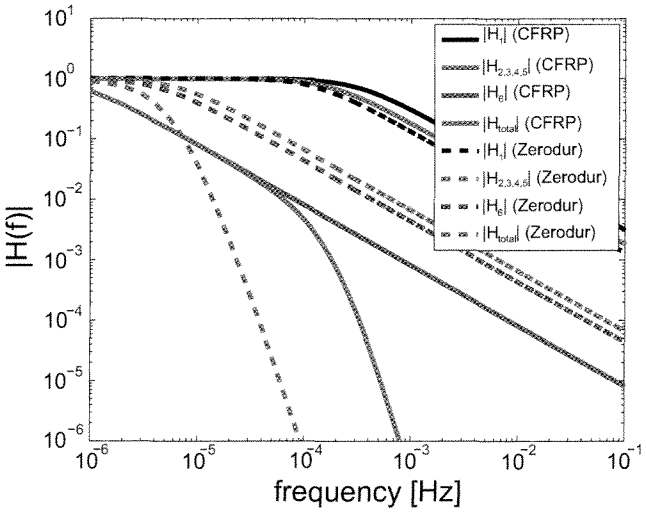

FIG. 16. Theoretical transfer functions for the CFRP (solid lines) and Zerodur (dashed lines) tanks.